Capacitive sensor for active tip clearance control in a palm-sized gas turbine generator

Tibor Fabian, Fritz Prinz Georg Brasseur, *Senior Member, IEEE*

***Abstract*—The efficiency of a gas turbine has an inverse relationship to the clearance between the rotor blades and the casing. Recent efforts in miniaturization of micro gas turbine engines have created a new challenge in blade tip clearance measurement. This paper describes the development of a capacitive tip clearance measurement system, based on a synchronous detection of a phase-modulated signal, for a palm-sized gas turbine engine with an integral ceramic rotor piece. A surface modification of the ceramic compressor and rotor with conductive coating is utilized to create a novel configuration of a tip clearance probe. The probe capacitance varies by approximately 120 fF for a 100 μm blade displacement. Periodic auto-calibration is used to reduce the effects of temperature drift on the sensor output. The remaining measurement error drift of 1.5 fF/°C was caused by the temperature drift of the probe parasitic capacitor. The random uncertainty was between 1.9 μm and 6.9 μm depending on the tip clearance gap.**

***Index Terms*—micro gas turbine, blade tip clearance, capacitive sensor**

I. Introduction

Continuous demand for self-powered applications has prompted the development of portable high energy and high power density power supplies: batteries, supercapacitors and fuel cells. Another approach to micro-power source design attempts to scale down well-established, large-scale heat engines. Similar to fuel cells, they operate on hydrocarbon fuels with energy densities of approximately 40 MJ/kg. Unlike fuel cells, their thermal efficiency is limited by the Carnot cycle. Additionally, the energy conversion occurs in two steps: first from chemical to mechanical energy and then from mechanical to electrical energy, thus introducing losses and further reducing overall efficiency. Nevertheless, the efficient operation of a fuel cell requires many auxiliary devices (e.g., humidifiers, pumps), which are not easily scaled down and, consequently, they reduce the efficiency and power density of miniature fuel cells.

Several concepts for miniature heat engines with output power up to tens of watts are being explored [1], in particular: miniature gas turbines [2], Striling cycle machines [3], Wankel rotary engines [4], and nontraditional engines [5].

The Rapid Prototyping Laboratory at Stanford University is developing a palm-sized gas-turbine generator. The engine is roughly 3 cm in diameter and 8 cm long. The engine consists of a gas-generator and an electric alternator linked together by a single rotor piece. The rotor consists of a radial inlet turbine arranged back-to-back with a centrifugal compressor impeller, and a rotor shaft extension housing a permanent magnet (see Fig. 1). The rotating shaft is supported on two hybrid ceramic ball bearings or, equivalently, on air bearings. The rotor group is axially constrained with a thrust bearing at the end of the rotor shaft. According to the design analysis, an electric output power of 100 W can be achieved with an turbine inlet temperature of 1050 °C and a radial flow compressor impeller with 12 mm diameter spinning at 800,000 rpm.

The downsizing of the gas-turbine has significant implications for material selection. Smaller machines tend to operate at higher frequencies compared to their large-scale counterparts. Increased rotational frequency is associated with higher acceleration and hence higher loads on structural elements. Given that the efficiency of heat engines can be improved at elevated temperatures, the availability of a proper high temperature material for the turbine becomes a crucial issue.

Engineering ceramics are an obvious material candidate for turbine manufacture. Ceramic materials are known to survive extreme temperatures conditions, yet they suffer from inherent brittleness caused by atomic defects or macroscopic voids and inclusions. In the present project, we have adopted silicon nitride as the material of choice, since appropriate 3D fabrication methods (mold SDM [6]) are now available to manufacture engine components with characteristic feature sizes of less than 200 μm. Ceramics have another distinct advantage over metal in their low coefficient of thermal expansion, which is particularly attractive in applications where a high temperature gradient occurs, such as in a small gas turbine engine.

Efficiency is an important performance parameter of gas turbine engines. The losses occurring in turbomachinery are usually divided into several categories. Most of the losses can be optimized by the use of computational design methods; however, the leakage loss caused by the presence of a physical gap between the stationary shroud and the rotating blades cannot be improved by aerodynamic design [7].

The effect of the physical gap on the efficiency of large-scale turbines has been previously studied, and the gap efficiency relationship is typically stated as an empirical formula. In the case of unshrouded compressors, Pampreen [8], Eckert and Schnell [9], and Pfleiderer [10] suggest the following formula

$$-\frac{\Delta\eta_{comp}}{\eta_{comp,0}} = \frac{2ac_2}{b_1 + b_2}. \quad (1)$$

Here $\eta_{comp,0}$ is the compressor efficiency at zero tip clearance, $\Delta\eta_{comp}$ is the efficiency change, b_2 is the blade height

Department of Mechanical Engineering
Stanford University, Stanford CA, 94305, USA
Phone: (650) 723-1138, email: tfabian@stanford.edu
Institute of Electrical Measurement and Measurement Signal Processing
Graz University of Technology
Kopernikusgasse 24/4, A-8010 Graz, Austria

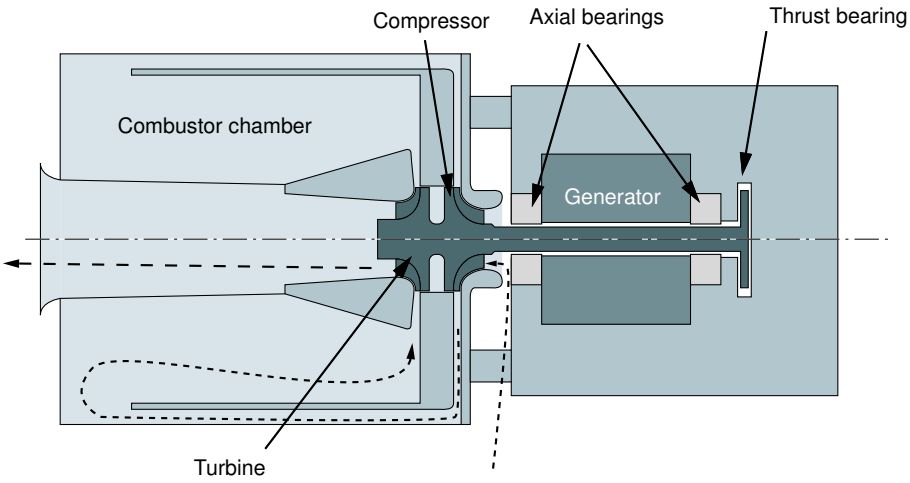

Fig. 1. Schematic cut-away view of the micro-gas turbine built at RPL, with air flow visualized by a dashed line.

at the outlet, b_1 is the blade height at inlet, c_2 is the tip clearance at the compressor outlet, and a is an empirical constant, with suggested values between $a = 0.9$ to $a = 3$ (see Fig. 2).

The effect of the tip clearance on the efficiency of a micro gas turbine is similar to the effect in large-scale turbomachinery. If we substitute the dimensions and parameters of the compressor shown in Fig. 2, namely, $a = 0.9$, $b_1 = 1$ mm, $b_2 = 0.8$ mm, $\eta_{comp,0} = 71$ %, into Eq. (1), then, at a nominal operating tip clearance of 75 μm, the compressor efficiency is expected to drop by 6 percentage points; further increase of the tip clearance by a 50 μm reduces the compressor efficiency by an additional 3 percentage points. Kang [11] performed a set of spin rig tests with the micro gas turbine compressor illustrated in Fig. 1 at a reduced speed of 440 krpm. The effects of the 50 μm gap variation resulted in an approximately 3 percentage points drop of compressor adiabatic efficiency.

Small variations in compressor efficiency have a large impact on the electrical power output of the micro gas turbine generator. In a feasibility study of an 100 W-sized micro gas turbine engine, Isomura [12] showed the dramatic impact of the compressor efficiency on the generated power output. According to the study, a 10 percentage points variation in the compressor efficiency results in a 75 W change in output power, which may render the design of the micro gas turbine generator unfeasible and highlights the importance of high compressor efficiency.

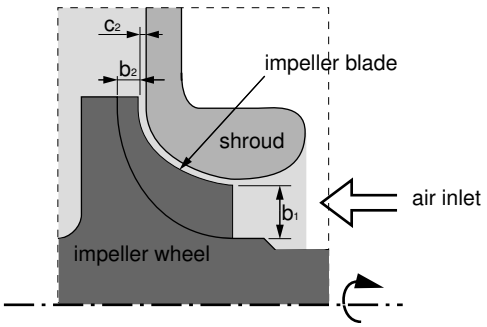

Fig. 2. Simplified sectional view of compressor-turbine rotor group and compressor casing.

Minimum tip clearance is desired for highest compressor efficiency. Unfortunately, due to manufacturing tolerances, complex modes of thermal expansion, vibrations, and time varying loading, the tip clearance can significantly change during gas turbine operation. Typically, at some point of the operation, the gas turbine experiences a "pinch point" at which the tip clearance reaches its minimum, and rubbing between the tips of the rotating blades and stationary shroud may occur. This in turn may lead to rotor destruction. To prevent rotor damage, turbine designers typically set the tip clearance at the pinch point to some safe minimum, consequently increasing the tip clearance during the rest of the turbine operation. An active tip clearance control system that maintains a constant tip clearance during the entire operation can therefore improve the performance of the gas turbine.

This paper describes the design of an active tip clearance control system for a micro-gas turbine engine with an unitary ceramic shaft. In particular, this paper presents the actuation scheme, the design of air-gap coupled electrodes for a capacitive tip clearance sensor, the auto-calibration measurement of the tip clearance capacitance, practical implementation of the capacitance sensor based on a synchronous detection of a phase modulated signal, and results obtained from a cold air test-rig.

II. Actuation scheme

The purpose of the active control system is to compensate for the expected variation of the tip clearance during the gas turbine operation. The dominant cause of tip clearance variation in the micro-gas turbine is the thermal expansion mismatch of different engine components. In particular, the largest dimensional change occurs in the axial direction. The turbine design depicted in Fig. 1 makes access to the tip clearance gap of the turbine section impossible, since the turbine wheel is completely surrounded

by the annular combustion chamber containing combustion gasses at 1050 °C. Therefore, we have decided to control the tip clearance in the compressor section with the benefit of a reduced temperature in the tip clearance gap.

There are many patents describing large-scale blade tip clearance control concepts. Lattime et al. [13] divided these concepts into five major categories: active thermal, active mechanical, passive thermal, active pneumatic, and passive pneumatic. Only the active concepts are of interest for us. Active thermal concepts use compressor air to thermally expand or contract segments of the shroud. The drawback is the slow thermal response and compressor air bleed, which reduces efficiency. The active mechanical concepts typically combine linkages and actuation to vary the tip clearance. The limiting factor for this concept is the lack of high temperature actuators, which results in the use of linkages and thus increases mechanical complexity and weight. The active pneumatic designs use engine pressure to load deflectable shroud segments. The drawback of this method is the bleed of engine pressure that could reduce the efficiency and sensitivity to pressure balancing.

The downsizing of the engine and the constrained space around the compressor inlet prohibit the use of complex mechanical actuation concepts; similarly, the active thermal design is unfeasible since it would reduce the turbine efficiency and cannot compensate for large axial offsets. However, the unique design of the rotor group makes it possible to use an active mechanical design without the need for a high temperature actuator or complex mechanical linkages.

In a centrifugal compressor, the gap clearance along the blade changes from radial at the inlet to axial at the outlet. The proposed actuator scheme controls the axial tip clearance at the outlet of the compressor by monitoring the axial tip clearance with an appropriate sensor and adjusting the tip clearance by displacing the entire rotor group in the axial direction. The fact that the rotor group is supported radially by air-bearings and axially by a thrust bearing makes it possible to control the axial rotor displacement by acting on the thrust bearing. Since the thrust bearing is located at the cold end of the generator (see Fig. 1), the temperature requirements for the actuator are minimized.

In conclusion, the proposed active tip clearance concept controls the compressor efficiency by axially displacing the unitary rotor piece through an actuator, which controls the axial position of the stationary part of the thrust bearing. Hence, this control scheme can be implemented the best with a tip clearance sensor that measures the average axial tip clearance, ergo the average blade tip clearance at the outlet of the compressor.

III. Previous work

Many sensing principles have been used for tip clearance measurements in large-scale turbomachinery: optical, capacitive, electromechanical, hybrid capacitive and electromechanical, magnetic, eddy-current, microwave, ultrasound, and fluidic.

The optical sensors can be further divided into triangulation [14], line of sight [15], astigmatic [16], [17], fiber optic proximity [18], and time-of-flight techniques [19]. In general, the optical sensors can attain the best resolution (triangulation method) and the highest system bandwidth; however, compared to other sensors, they are often complex, bulky, expensive, contain alignment sensitive elements, and are sensitive to contamination.

Several capacitance detection techniques have been applied to measure the variable blade tip capacitance: FM modulation [20], AM modulation [21], phase modulation [22], charge amplifiers [23] and variable amplifier feedback [24]. Capacitive sensors suffer from low spatial resolution, short measurement range, and need for calibration, but are popular due to their simplicity, low cost, and robustness.

Electromechanical systems [25] belong to the oldest blade tip clearance measurement systems. The main benefit of a blade tip clearance sensor based on the electromechanical principle is its high resolution over the entire measurement range. Its drawbacks are the tip clearance measurement of only the longest blade, slow response time, and the probe tip's susceptibility to mechanical damage during fast, large-scale blade transients.

Hybrid capacitive-electromechanical sensors [26] combine the strengths of capacitive and electromechanical techniques into one probe: the high accuracy of the longest blade detection and the good resolution at small gap clearances of a capacitive sensor. Thus, the hybrid sensor has the advantage of auto-calibration, but, at the same time, it is bulky and complex.

Variable reluctance and eddy current sensors are also used to detect blade tip clearance. The drawback of variable reluctance sensors [27] is the fact that the output signal depends not only on the gap but also on blade speed and temperature. The drawback of the eddy current sensors [28], [29] is the complex dependence of sensor output on the gap and bad scaling of the sensing coil. As the coil size decreases, the parasitic resistance increases and reduces the sensor's sensitivity.

Microwave sensors [30], [31] are in general very robust and insensitive to contamination; however, due to the wave nature of the microwaves, the wavelength has to be scaled down with the blade thickness. Unfortunately, the hollow waveguides at the sub-millimeter wavelengths are impractical and the corresponding circuitry complex.

Pneumatic tip clearance sensors [32] are popular because of their insensitivity to the blade tip contamination and electromagnetic interference. Their drawbacks are diminishing signal strength with decreasing blade thickness, output dependence on the turbine operating conditions, and bandwidth limitations.

In the ultrasound sensors [33], similar to microwave sensors, the diffraction limitation caused by downsizing of the blade thickness can be avoided by increasing the operating frequency, which, however, increases the complexity of the receiver. Unlike the microwave sensors, the wave propagation of ultrasound depends on the temperature, pressure, and relative speed of the air in the gap. Thus, the op-

erating conditions of the engine significantly influence the sensor output.

The measurement of a tip clearance in a gas turbine is a challenging problem, and several techniques have been applied to solve this task. As a consequence of downsizing, none of the existing sensors can be directly used to measure the tip clearance in the micro-gas turbine environment. The size of most of the existing probes is larger than the micro-gas turbine itself. In addition, the use of nonconductive rotor materials prohibits the use of certain sensor techniques. Despite their drawbacks, the eddy-current, and the capacitive sensors have the best potential to be successfully adapted for the micro gas turbine environment. Because of its simple design, flexible miniaturization, and potential for improved performance through novel electrode configuration by selective conductive coating of the rotor blades, we have decided to investigate the capacitive sensor technique for average tip clearance measurement in a compressor environment of a miniature gas turbine.

IV. Electrode design

The traditional capacitive tip clearance sensor consists of a coaxial probe with a central electrode and one or more concentric electrodes [34], [35]. The relative dimensions of the center electrode, the concentric electrodes, and the blade width affect the probe performance, e.g., range, sensitivity, linearity. Typically, the probe range is given as a percentage of the probe diameter, hence the range will increase with increasing probe diameter. However, there is an upper limit to the probe diameter set either by the blade spacing or blade curvature.

The downsizing of the compressor leads to the downsizing of the measurement probe and consequently to the reduction of probe capacitance when scaled isotropically. An estimate of a probe capacitance variation for a coaxial probe design meeting the space restrictions of the compressor shroud shown in Fig. (2) was performed. Assuming electrically grounded metallic blades, a coaxial probe design, and a parallel plate capacitor formula a $\pm$ 50 μm variation of the tip clearance around the nominal tip clearance of 75 μm results in a 20 fF variation of tip clearance capacitance between the probe's center electrode and the blade. In this calculation, we have assumed that the blade curvature limited outer diameter of the coaxial sensor probe is 600 μm, center electrode diameter is 300 μm, and the width of the compressor blade is 300 μm. The resulting probe capacitance of a coaxial probe design is impractical. Furthermore, if the metallic blades are replaced with ceramic ones the already minuscule probe capacitance further decreases.

To increase the probe capacitance when used with ceramic blades, Barranger [36] proposed a conductive coating of the blade tips. First, all the blade tips were coated with a thin platinum film. Then, the tip coating was connected with an additional platinum strip to a metal shaft and grounded through metallic bearings supporting the rotor shaft. However, the rotor group of the investigated gas turbine, as shown in Fig. 1, is supported by non-conductive, high-speed bearings, based on air or ceramics ball support. In either case, the impedance between the conductively coated rotor and the ground is capacitive and not resistive. As a consequence, the application of a conductive coating on the all ceramic rotor resulted in a tip clearance capacitance between the center probe electrode and electrically floating rotor coating in series with an undefined capacitance between the rotor coating and electrical ground. Consequently, the minuscule probe capacitance was further reduced by the presence of the undefined coupling capacitor in series with the center electrode capacitance.

Figure 3 shows schematically an electrode configuration that overcomes the disadvantages of a coaxial probe configuration that detects conductively coated blades. A section of the originally nonconductive rotor assembly is patterned with a conductive coating. The coating extends from the compressor surface towards the generator, past the compressor inlet. The conductive compressor surface and the conductive and electrically grounded compressor shroud form the electrodes of the tip clearance capacitor, C_{tc}, while the surface of the rotor shaft and a stationary coupling electrode form a well-defined, and axial displacement-insensitive, coupling capacitor, C_c, (see Fig. 3). Since capacitance, to a first approximation, is inversely proportional to the capacitor plate distance, only the blade tips contribute to the resulting capacitance C_{tc}. Therefore, the capacitance C_{tc} is the sum of capacitances of individual blades and thus linearly proportional to the average blade tip capacitance and, at the same time, one to two orders of magnitude larger than the tip clearance capacitance of a coaxial probe.

The coupling capacitance can inversely affect the sensor performance. The resulting probe capacitance, C_e, measured between the stationary electrode of the coupling capacitor, C_c, and the grounded shroud, equals the series combination of the coupling capacitance, C_c, and the tip clearance capacitance, C_{tc}: $C_e = \frac{C_{tc}C_c}{C_{tc}+C_c}$. Consequently, the probe capacitance, C_e, will be smaller than the tip clearance capacitance, C_{tc}, and a nonlinear function of both capacitances in series. The coupling capacitance, C_c, is formed by a coaxial structure along the rotating shaft and therefore is insensitive to axial displacement of the rotor group. However, the shaft vibration may cause a variation of the coupling capacitance C_c and therefore

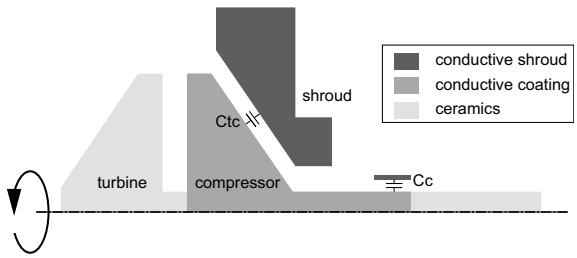

Fig. 3. Simplified sectional view of compressor-turbine rotor group and compressor casing with depicted surface modifications of the ceramic rotor and the resulting capacitors.

variations of the probe capacitance, C_e. This effect can be minimized by placing the coupling capacitor immediately next to the axial bearing supporting the rotor. Additionally, the radial shaft vibrations are proportional to the rotational speed and thus the corresponding signal variations are in a much higher frequency range than the thermal tip clearance variations and can be suppressed by filtering.

V. Sensing circuitry

The proposed sensor, similar to the design presented by Demers [37], is based on a phase modulation of a constant frequency reference oscillator by de-tuning of a parallel resonant circuit with a load capacitance. The impedance of a parallel resonance circuit is purely resistive when driven at the resonant frequency and has non-zero reactive component if driven outside of resonance. Therefore, the phase of the complex impedance will be zero at resonance and nonzero outside. A change in the resonant circuit parallel capacitance will de-tune the circuit and cause a phase shift that can be measured and facilitated to determine the capacitance change.

The basic building blocks of the circuit are shown in Fig. 4. It consists of a reference oscillator, a tuned parallel resonant circuit, a set of three analog switches, a probe capacitor, two reference capacitors, a microcontroller, a digital to analog converter, and a phase detector comprised of two comparators, an analog mixer, and a low-pass filter. The purpose of the comparators in the phase detector is to remove the dependency of the output signal on the input signal amplitude and to linearize the dependency of the phase detector output on the phase difference of the input signals. The probe tip capacitor and two reference capacitors are individually connected to the parallel resonant circuit through analog switches $S1$, $S2$, and $S3$. A reference oscillator feeds the capacitively coupled resonant circuit. The phase detector shown in Fig. 4 transforms the phase difference of the signals at the comparator inputs into voltage with zero volt output when the comparator input voltages are phase shifted by 90°.

In resonance, the phase of a parallel resonant circuit is zero, hence, for a zero volt phase detector output a 90° phase-shifted version of the reference signal is needed. In previously reported work [38], the phase-shifted signal was obtained with a dedicated 90° phase-shifting network. However, phase shifting networks typically increase circuit complexity or the resulting phase-shift is frequency dependent. In the circuit shown in Fig. 4 the voltage across the resonant circuit is compared with the voltage across the coupling capacitor. In resonance, the parallel resonant circuit is purely resistive and the voltage across the resonant circuit is therefore 90° phase-shifted relative to the voltage across the coupling capacitor [39].

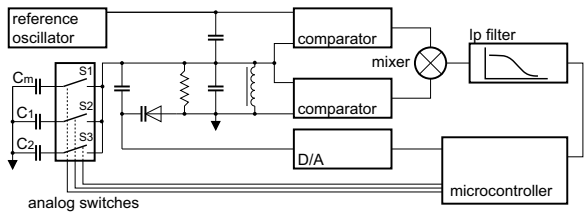

Fig. 4. Block diagram of the sensor circuitry. It consists of a reference oscillator, a capacitively coupled tuned resonant circuit, a phase detector, a set of three analog switches, and a microcontroller.

The circuit elements of the tuned resonant circuit are subject to environmentally induced variations affecting the output of the phase detector. These effects are suppressed by an auto-calibration procedure described in section VII. The best error correction by the auto-calibration is achieved when the resonant circuit is operated close to the resonance condition. Hence, the resonant circuit is periodically re-tuned with a reverse biased PN junction diode, a varactor. The varactor tuning voltage is controlled by a microcontroller driven D/A converter.

While in operation, the microcontroller periodically calculates a new clearance value. A single output value is obtained by a sequence of steps. First, the reference capacitance C_1 is connected to the resonant circuit: the analog switch $S2$ is turned on and the analog switches $S1$, and $S3$ are turned off. After the phase detector output has stabilized, it is sampled, averaged and the digital value is stored. This step is then repeated for C_2 and C_m. Second, based on the phase detector output for the reference capacitors and a known phase detector output for the resonance condition, a new value of the varactor tuning voltage is calculated and the output of the D/A converter is updated. Third, an estimate of the tip clearance capacitance based on the auto-calibration algorithm is calculated. At last, the tip clearance capacitance is converted into the tip clearance with the help of a calibration curve. A sketch of the voltage output of the phase detector during single measurement sequence is shown in Fig. 5.

The varactor voltage is always adjusted in a manner that minimizes the nonlinear effects of the phase-capacitance curve of the tank circuit. The compensation properties of the auto-calibration algorithm require that the system is linear for all three capacitance measurements. The reference capacitors C_1, C_2 are selected so that the probe capacitance is, in the entire measurement range, smaller then C_2 and larger then C_1: $C1 < C_m(c) < C_2$. Then the varactor tuning voltage is adjusted until the phase of the tank circuit when individually loaded by the reference capaci-

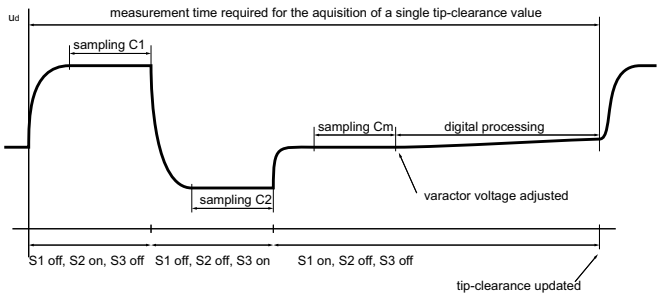

Fig. 5. Sketch of a sensor output during the time required to acquire a single tip-clearance value.

tors $C1$ and C_2 has the same absolute value but opposite sign.

Note that the periodic tuning of the resonant circuit with the varactor does not interfere with the three capacitance measurements, since the varactor voltage is held constant during the three measurements. The varactor voltage is updated only once during a single measurement period after the three capacitors were sampled. The next measurement sequence doesn't start until the microcontroller performs the auto-calibration operation with the sampled values. During this time the phase detector output can stabilize.

VI. Circuit analysis

Figure 6 is the equivalent network of the tuned resonant circuit. The inductor is approximated by a network consisting of an ideal coil with a total inductance L_s in series with a resistance R_{ls} and a shunt capacitance C_{lp}. The series resistance, R_{ls}, represents the winding as well as the core losses. Both types of losses are frequency dependent due to the eddy-currents.

The reference oscillator is represented by the output impedance, R_g, of the buffer stage driving the capacitor C_{cr} in series with the resonant circuit. The input impedance of the comparator is considered to be a parallel combination of an input capacitance, C_{ci}, and an input resistance, R_{ci}. Each of the three analog switches $S1$, $S2$, and $S3$, is approximated by a device consisting of an ideal switch in series with a series resistance, R_{ss}, and having an input as well as an output impedance modelled as a parallel combination of a resistance and a capacitance, R_{si}, C_{si} and R_{so}, C_{so}.

The output resistance, R_{so}, as well as the output capacitance, C_{so}, of the three analog switches are well matched among the switches since they are located on the same integrated circuit, as shown in section IX. The output capacitance C_{so} is additionally increased by a board capacitance of the pads and traces required to connect the measurement capacitors to the analog switches. Thanks to the symmetric board layout, the board parasitic capacitances at the switch output are considered identical. However, the probe capacitance, C_e, is in parallel with a large parasitic capacitance, C_o, of the conductor (board traces, coaxial cables, etc.) connecting the probe capacitor to the switch.

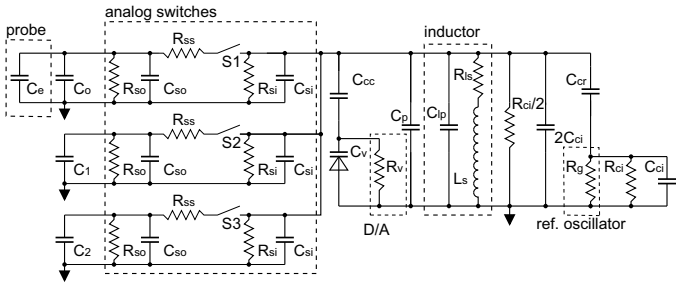

Fig. 6. Equivalent electrical network of components forming the tuned resonant circuit in Fig. 4

The buffer stage, driving the varactor with the tuning voltage from the D/A converter, is represented by a resistance R_v, and the varactor diode is connected to the resonant circuit by a large coupling capacitor, C_{cc}. The capacitance between the circuit traces and a ground layer of the printed circuit board adds to the total capacitance and is modelled by a board parasitic capacitance, C_p.

The number of factors in the equations describing the circuit can be reduced by first converting all circuit elements into their equivalent parallel representation and then lumping alike components together. Figure 7 shows the reduced equivalent network.

The quality of the coil, Q_l, is typically sufficiently large, $Q_l \geq 10$, and hence the parallel equivalent inductance, L_t, is in a good approximation equal to the series inductance, L_s:

$$L_t = L_s. \tag{2}$$

The total parallel resistance as well as the parallel capacitance of the tuned resonant circuit depend on the state of the three analog switches. As explained in section V, at any instance during the measurement only one switch is on and the others are off. Since the output switch resistance, R_{so}, is assumed identical for all three switches, the total parallel resistance, R_t, of the resonant circuit is identical for all three measurements, where

$$\frac{1}{R_t} = \frac{1}{R_v} + \frac{1}{R_{lp}} + \frac{3}{R_{si}} + \frac{1}{R_{so}} + \frac{2}{R_{ci}}. \tag{3}$$

Here, R_{lp} is the equivalent parallel resistance of the coil including both the core and the skin-effect losses. The effects of the switch series resistance, R_{ss}, the output resistance of the reference oscillator buffer stage, R_g, as well as the input impedance of the comparator connected to the reference oscillator output were neglected.

The parallel capacitance of the resonant circuit will change during the measurement sequence. However, we can lump together capacitances that are identical for all three measurements into a tank capacitance, C_t, and the variable capacitance into a loading capacitance, C_l, where

$$C_t = 3C_{si} + C_{so} + C_p + C_{lp} + C_v + 2C_{ci} \tag{4}$$

and

$$C_l \in \{C_m, C_1, C_2\}. \tag{5}$$

When the switch $S1$ is on, the loading capacitance, C_l, equals the probe capacitance, C_e, enlarged by the offset capacitance C_o. The resulting capacitance is denoted as C_m: $C_m = C_e + C_o$.

The phase, ϕ_r, of the parallel resonant circuit complex impedance equals

$$\phi_r(C_l + C_t) = -arctan\left(R_t(\omega_g(C_t + C_l) - \frac{1}{\omega_g L_t})\right) \tag{6}$$

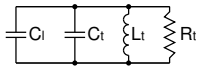

Fig. 7. Simplified equivalent electrical network of Fig. 6

where ω_g is the signal frequency of the reference generator. The voltage output of the phase detector, u_d, is linearly proportional to the phase of the resonant circuit impedance

$$u_d(C_t+C_l) = k_d * arctan(R_t(\omega_g(C_t+C_l) - \frac{1}{\omega_g L_t})) + u_o. \quad (7)$$

Here, u_o is a voltage offset needed to adjust the phase detector output to the A/D converter input range of the microcontroller, and k_d is a proportionality factor determined by both comparator voltage levels and signal amplification after phase detector.

VII. Auto-calibration

Several types of errors can be compensated for by a 3-point auto-calibration [40]. For a simplicity in notation let us assume a linear transducer that converts an unknown measurand, x_m, into an electrical signal, y_m, where

$$y_m = bx_m + a, \quad (8)$$

and a, b are transducer dependent parameters. By performing two additional measurements y_1, y_2 with two reference measurands x_1, x_2, $(x_2 > x_m > x_1)$, we can estimate the measurand x_m with the following formula:

$$\hat{x}_m = x_{1c} + \frac{y_m - y_1}{y_2 - y_1}(x_{2c} - x_{1c}). \quad (9)$$

The quantities x_{1c}, x_{2c} are assumed values of the reference measurands x_1, x_2 obtained by reference measurement equipment prior to the sensor operation. This 3-point auto-calibration reduces the sensor output dependency on the transducer parameters, as will be shown in section VIII.

The phase detector signal according to Eq. (7) can be approximated as linearly proportional to the loading capacitance C_l. The arctan function shows the largest slope and a good linearity for arguments close to zero. Hence, for the tuned circuit capacitances, $C_t + C_l$, close to the resonant condition capacitance, C_r, the transducer output is in a good approximation linearly proportional to the loadin capacitance:

$$u_d(C_l + C_t) = k_d \omega_g R_t (C_l + C_t - C_r) + u_o. \quad (10)$$

This approximation deviates from the actual value in Eq. (7) by less than 1 % for

$$|\omega_g R_t (C_l + C_t - C_r)| \leq 0.2. \quad (11)$$

Hence, the probe capacitance estimate, $\hat{C}_e$, obtained by substituting capacitances $C_1 + C_t$, $C_2 + C_t$, $C_e + C_o + C_t$ for measurands x_1, x_2, x_m, the phase detector output, u_d, for the transducer output, y, and Eq. (10) for u_d into Eq. (9), yields

$$\hat{C}_e = C_{1c} + \frac{C_m - C_1}{C_2 - C_1}(C_{2c} - C_{1c}) - C_{oc}, \quad (12)$$

where C_{1c}, C_{2c}, and C_{oc} are the values of C_1, C_2, and C_o determined by reference measurement equipment during an initial calibration prior to the operation of the sensor.

The probe capacitance, C_e, is in general a nonlinear function of the tip clearance, c, and the exact relationship is determined by a calibration function f_c: $\hat{C}_e = f_c(c)$. Consequently, the tip clearance estimate, $\hat{c}$, is determined by an inverse of the calibration function f_c:

$$\hat{c} = f_c^{-1}(\hat{C}_e) \quad (13)$$

VIII. Measurement errors

A. Systematic errors

The accuracy of the sensor will be limited by systematic and random errors. The major source of systematic errors is the drift of sensor components, e.g., due to changes in ambient temperature.

The calibration process is depicted graphically in Fig. 8. The actual values of the reference measurands x_1, x_2 differ from the assumed values x_{1c}, x_{2c}. Consequently, the measurand estimate $\hat{x}_m$ will differ from the actual measurand x_m. The measurement error, Δx_m, can be expressed as the difference between the measurand estimate $\hat{x}_m$ and the actual measurand x_m

$$\Delta x_m = \hat{x}_m - x_m. \quad (14)$$

The actual measurand x_m can be expressed as

$$x_m = x_1 + \frac{y_m - y_1}{y_2 - y_1}(x_2 - x_1). \quad (15)$$

Substituting Equations (15), (9) into Eq. (14) yields

$$\Delta x_m = \Delta x_1 \frac{x_{2c} - \hat{x}_m}{x_{2c} - x_{1c}} + \Delta x_2 \frac{\hat{x}_m - x_{1c}}{x_{2c} - x_{1c}}, \quad (16)$$

where $\Delta x_1 = x_{1c} - x_1$ and $\Delta x_2 = x_{2c} - x_2$.

Substituting C for x into Eq. (16) and expressing errors as relative errors yields

$$\begin{aligned} \Delta C_e = & \frac{\Delta C_1}{C_{1c}} \frac{C_{1c}(C_{2c} - \hat{C}_m)}{C_{2c} - C_{1c}} \\ & + \frac{\Delta C_2}{C_{2c}} \frac{C_{2c}(\hat{C}_m - C_{1c})}{C_{2c} - C_{1c}} - C_{oc} \frac{\Delta C_o}{C_{oc}} \end{aligned} \quad (17)$$

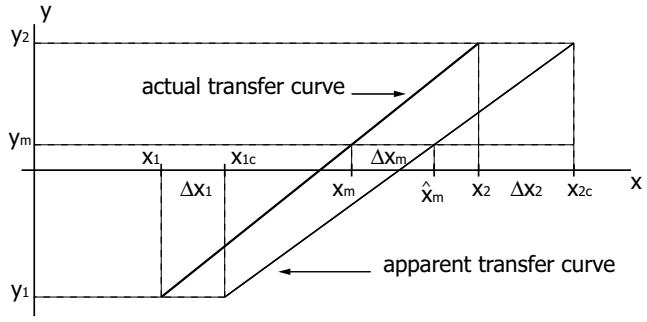

Fig. 8. Graphical representation of the calibration process with depicted measurement error, Δx_m, as well as calibration errors Δx_1, Δx_2.

Assuming the temperature drift of both reference capacitors is equal

$$\frac{\frac{\Delta C_1}{C_{1c}}}{\Delta T} = \frac{\frac{\Delta C_2}{C_{2c}}}{\Delta T} = \frac{\frac{\Delta C}{C}}{\Delta T} \tag{18}$$

the capacitance measurement error drift becomes:

$$\frac{\Delta C_e}{\Delta T} = \hat{C}_e \frac{\frac{\Delta C}{C}}{\Delta T} + C_{oc}\left[\frac{\frac{\Delta C}{C}}{\Delta T} - \frac{\frac{\Delta C_o}{C_o}}{\Delta T}\right] \tag{19}$$

and the tip clearance measurement error drift is

$$\frac{\Delta c}{\Delta T} = \frac{df^{-1}(\hat{C}_e)}{dC}\left(\frac{\Delta C_e}{\Delta T}\right). \tag{20}$$

As can be seen, a complete drift compensation is impossible since the drift is a function of the measurand estimate $\hat{C}_e$. However, it is possible to eliminate the effect of the board capacitance drift on the measurement error drift by constructing both reference capacitors C_1, C_2 as a parallel combination of a high-drift board capacitor of the same size and exposed to the same temperature changes as C_o and a low-drift reference capacitor. Hence, $C_1 = C_1' + C_o$ and $C_2 = C_2' + C_o$, where C_1' and C_2' are low-drift reference capacitors. Substituting for C_1 and C_2 into Eq. (17) and assuming equal temperature drift for the new reference capacitors C_1' and C_2' the measurement error drift becomes

$$\frac{\Delta C_e}{\Delta T} = \hat{C}_e \frac{\frac{\Delta C}{C}}{\Delta T}. \tag{21}$$

Consequently, with a careful matching of the parasitic board capacitances arranged in parallel with the reference and the probe capacitors, the board capacitance drift can be suppressed and the remaining drift is caused solely by the drift of the reference capacitors.

In summary, the 3-point auto-calibration can suppress the effects of the transducer parameters on sensor output if the transducer output is described by a first-order polynomial with respect to the measurand and if the change in the transducer parameters is negligible during the time required to perform the measurements of C_m, C_1, and C_2. The remaining measurement error is caused by calibration errors and drift of the reference and parasitic board capacitors.

B. Random errors

The second factor contributing to the total measurement uncertainty are random errors. These errors are caused by the presence of noise in the sampled signal. The uncertainty of the estimate $\hat{x}_m$ due to the random errors in the phase detector output depends on the exact timing as well as sequence in which the signals y_1, y_2, and y_m are sampled. The uncertainty also depends on the number of samples used for averaging and the shape of the power spectral density of the noise signal. However, the estimate uncertainty $\delta\hat{x}_m$ has an upper limit [41]

$$\delta x_{m,rnd} \leq \left|\frac{\delta x_m}{\delta y_1}\right|\sigma_{y_1} + \left|\frac{\delta x_m}{\delta y_2}\right|\sigma_{y_2} + \left|\frac{\delta x_m}{\delta y_m}\right|\sigma_{y_m}. \tag{22}$$

Here σ_{y_1}, σ_{y_2}, σ_y are the standard deviations of the phase detector output at different switch configurations. We have assumed that the process characterizing the phase detector output noise is stationary and independent of the analog switch configuration, hence, $\sigma_{y_1} = \sigma_{y_2} = \sigma_{y_m} = \sigma_y$. Then, simplifying Eq. (22) and substituting C_2, C_1, C_m for x_2, x_1, x_m, and u_d for y yields

$$\delta\hat{C}_{e,rnd} \leq \frac{2\sigma_{u_d}}{k_d \omega_g R_t}. \tag{23}$$

The linearity requirement limits the $\omega_g R_t$ term for a given maximum probe capacitance variation; hence, the estimate uncertainty can be reduced by increasing the amplification k_d. However, this will only reduce noise components introduced after the amplification stage, e.g, quantization noise. Any noise introduced prior to the phase detector, e.g., phase noise, will not be affected by a change of amplification, since it will be amplified with the signal. The last parameter determining the estimate uncertainty is the system bandwidth. The upper frequency is given by the cut-off frequency of the low-pass filter after the analog mixer, and the lower frequency is given by a fraction of frequency whose period is equal to the time required to obtain values $u_d(C_m)$, $u_d(C_1)$, and $u_d(C_2)$. The low frequency cut-off is a consequence of the error correction properties of the auto-calibration algorithm as explained in the previous section.

IX. Implementation

The tip clearance sensor, as shown in Fig. 4, was implemented in two units. The first unit contained a microcontroller (Motorola 68HC912 evaluation board) and the second analog unit contained all the analog circuitry except the reference oscillator. During the entire testing, an external signal generator (Agilent Technologies 8648B synthesized RF signal generator) was used as a reference oscillator. The analog unit was built on a single printed circuit board (PCB), which was also used as the stationary electrode of the electrode coupling capacitor, C_c. A conductively coated edge of a semicircular cut-out in the analog PCB was arranged concentrically with the rotor shaft, close to the compressor inlet, opposing the conductive coating on the rotor shaft, and forming a 50 μm radial gap. Consequently, the conductive edge of the analog PCB semicircular cut-out and the opposing conductive coating of the rotor formed a concentric-plate electrode coupling capacitor, C_c (see Fig. 9).

The resonant circuit was formed by an inductor in parallel with a reverse biased varactor diode (Zetex ZMV930 variable capacitance diode). The inductor was built with 42 windings of AWG 33 insulated copper wire on a toroid core (Micrometals T25-6 iron powder core). Three analog switches located on a single integrated circuit (Maxim MAX4545 quad bidirectional RF switch) connected the probe capacitance, C_e, as well as the two reference capacitors, C_1, C_2, to the inductor. The resonant circuit was capacitively driven, and the voltages across the resonant circuit coupling capacitor, C_{cr}, and the resonant cir-

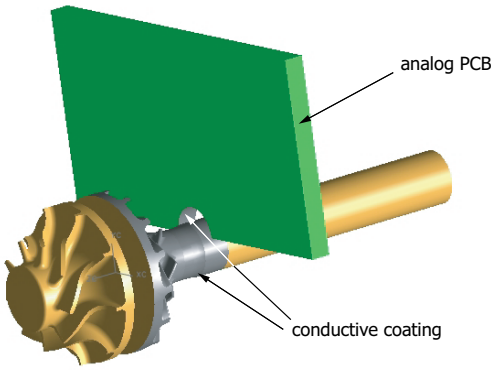

Fig. 9. Exploded view of the rotor group and the analog PCB with the semicircular cut-out forming the coupling capacitor. The inner face of the cut-out as well as the concentrically arranged rotor shaft are conductively coated. The diameter of the shaft is 4mm.

cuit itself were fed into two comparators (Analog Devices AD6687 ultra-fast comparator). The comparator outputs were then fed into the inputs of an analog multiplier (Analog Devices AD835, 250 MHz 4-quadrant voltage output multiplier), low-pass filtered with a 3 kHz analog filter, and digitized by a 10-bit A/D converter of the 68HC912 microcontroller.

The equivalent circuit shown in Fig. 6 is a simplified model of the resonant circuit elements and the component values are, in general, frequency dependent. Hence, all the component values have to be determined at the operating frequency. The implemented sensor was operated at 10 MHz. The inductance L_t was measured with an impedance analyzer (Solartron 1278) and was found to be 4.8 μH.

The tank capacitance, C_t, was determined by measurements of the tuned resonant circuit quality using a spectrum analyzer (Agilent E4402B) and an active FET probe (Tektronix P6243). C_t was found to be approximately 51.8 pF with 2.12 V across the varactor diode, Similarly, the tank resistance, R_t, was found to be 5 $k\Omega$.

The tip clearance capacitance, C_{tc}, as a function of ± 50 μm axial rotor displacement around the nominal tip clearance of 75 μm was determined with a 3D finite element simulation to vary between 9 pF and 4.5 pF. The probe capacitance, C_m, as a function of the tip clearance, c, varied between 3.63 pF and 3.51 pF. The coupling capacitance, C_o, was about 1.25 pF and the board parasitic capacitance, C_o, was about 2.53 pF.

The reference capacitors were selected as $C_1 = 3.45\ pF < 3.51\ pF$, and $C_2 = 3.83\ pF > 3.63\ pF$. The resonant circuit coupling capacitance, C_{cr}=4.37 pF, was selected so that its impedance at resonance was as close as possible to the impedance of the resonant circuit at resonance, R_t.

The linearity requirement for effective auto-calibration error correction is satisfied if the largest deviation from the resonance condition through loading of the resonant circuit by the reference capacitors satisfies Eq. (11). As shown in section VIII B, maximizing the $\omega_g R_t$ term reduces the random uncertainty. This is achieved by the varactor tuning algorithm, which minimizes the phase deviation from the resonance condition for both reference capacitances by enforcing $\phi_r(C_1) = -\phi_r(C_2)$. Assuming a linear phase capacitance relationship and solving for C_r yields $C_r = C_t + 0.5(C_1 + C_2)$. Finally, substituting values used in the experiment into Eq. (11 yields

$$\omega_g R_t (C_2 - C_1) = 0.12 < 0.4, \tag{24}$$

Hence, within the measurement range the tuned circuit is linear with less than 1% error.

X. Results

The performance of the sensor was evaluated on a cold-air spin-rig. The test-rig consisted of a custom-made cold-air inlet nozzle, a compressor shroud, a bearing cartridge and a PCB adapter attached to a linear guide block displaced along the axial direction by a micrometer (see Fig. 10). The custom inlet nozzle was made out of plastic, hence it was not suitable for hot gasses. During testing, the rotor was driven by compressed cold air supplied through the inlet nozzle. With this set-up, rotor speeds up to 400,000 rpm were attained. The shroud, the bearing cartridge, and the PCB adapter were made in a split design enabling a simple assembly. Figure 11 shows the test rotor piece with bearing cartridge in the spin rig. In this photograph the inlet nozzle, the analog PCB, as well as the top halves of shroud and the cartridge adapter have been removed.

Figure 12 shows a typical calibration curve obtained at a constant temperature and with a stationary rotor. The zero clearance distance was set as the clearance immediately before mechanical contact between blades and shroud occurred. This clearance was determined by the eccentricity of the blades and misalignment of the rotor and shroud. The random probe capacitance estimate uncertainty was 4.8 fF. This translates into 1.9 μm clearance uncertainty at the smallest tip-clearance and 6.9 μm at the largest

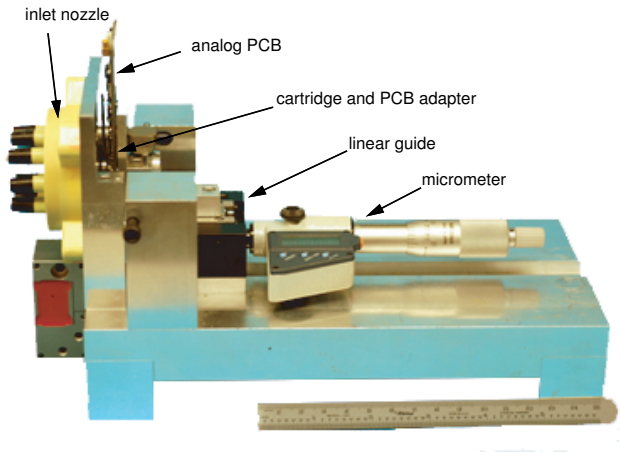

Fig. 10. Cold-air test rig consisting of an inlet nozzle, compressor shroud, rotor and a sensor PCB holder placed on a linear bearing and axially controlled by a micrometer.

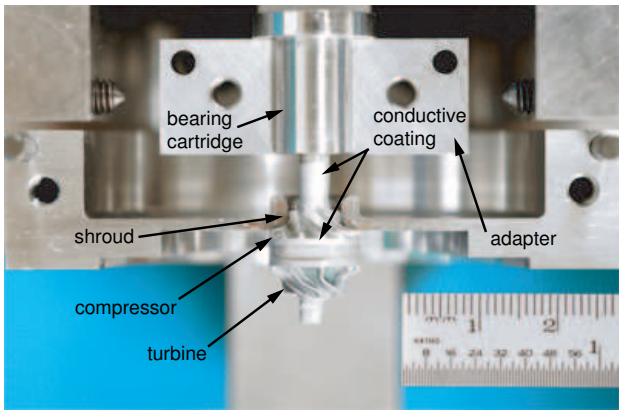

Fig. 11. Detail view of the rotor group in the test rig without nozzle, analog PCB, as well as upper halves of the shroud and rotor fixture.

tip clearance due to the changing slope of the calibration curve. The measurement error was dominated by the temperature drift of the board capacitance, C_o. The temperature coefficient of the reference capacitors was smaller than ± 30 $ppm/°C$ (NPO dielectric), while the temperature coefficient of the printed circuit board capacitance, C_o, was experimentally determined to be 900 $ppm/°C$. Substituting for the temperature drifts in Eq. (19) and assuming that the two drifts sum provides an estimated worst case temperature drift of 2.3 fF/°C and compares with the measured temperature drift of 1.5 fF/°C. The measurement temperature drift can be reduced by either minimizing the board capacitance, C_o, e.g., by active guarding, or by matching the parasitic board capacitances at the input of all three analog switches as was shown in section VIII

XI. Conclusions

The main conclusions of this paper are:

Small tip clearance variations of the micro-gas generator have a large impact on the power output and hence justify the need for active tip clearance control.

A simple active tip clearance control system can be implemented in the micro-gas turbine by axially displacing the unitary rotor piece through an actuator, which displaces the non-rotating part of the thrust bearing. This system requires an axial tip clearance sensor.

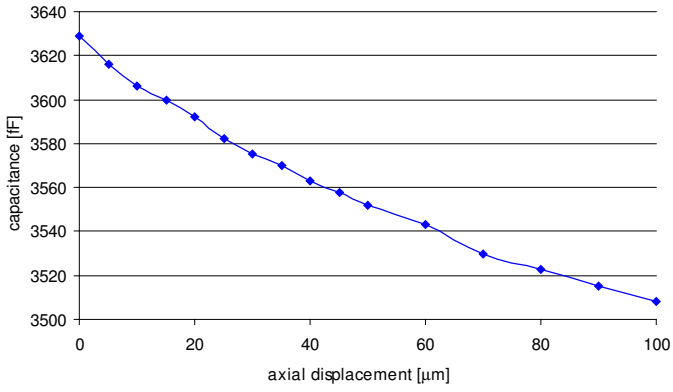

Fig. 12. Capacitance C_m at the input of the analog switch $S1$ as a function of the axial displacement, c, at room temperature and with stationary rotor.

The downsizing of a gas-turbine prevents a direct implementation of existing tip clearance sensors. Despite their drawbacks the eddy-current and the capacitive sensors have the best potential to be successfully adapted for the micro gas turbine environment.

Compared to the existing probes used to capacitively measure the tip clearance of ceramic blades, the proposed capacitive probe is an order of magnitude more sensitive.

A sensor based on a synchronous detection of a phase modulated signal can detect the approximately 120 fF capacitance change due to the blade gap variation of 100 μm. Periodic tuning, auto-calibration and compensation can minimize the effects of drift on the measurement error.

XII. Acknowledgments

The authors wish to thank Prof. J. P. Johnston for the design of the inlet nozzle and Dr. S. Kang for the manufacturing of the inlet nozzle and the ceramic rotor. The authors would like to gratefully acknowledge advice and help of Dr. H. Tsuru. Thanks are also due to T. Hasler for his contribution to the manufacturing of the engine test-rig. Authors are indebted to the reviewers for valuable comments and suggestions during the preparation of the manuscript.

References

[1] R. B. Peterson, "Small Packages," *Mechanical Engineering*, vol. 123, no. 6, pp. 58–61, June 2001.

[2] A.H. Epstein et al., "Shirtbutton-sized gas turbine: The engineering challenges of Micro High Speed Rotating Machinery," in *The 8th International Symposium on Transport Phenomena and Dynamics of Rotating Machinery (ISTROMAC 8)*, 2000.

[3] Garry Proulx, "Stirling cycle efforts," in *High Energy Density/High Power Density Power Sources, Prospector III*, 1992, pp. 461–470.

[4] K. Fu, A.J. Knobloch, F.C. Martinez, D.C. Walther, C. Fernandez-Pello, A.P. Pisano, and D. Liepmann, "Design and fabrication of a silicon-based mems rotary engine.," in *Micro-Electro-Mechanical Systems (MEMS). 2000 ASME International Mechanical Engineering Congress and Exposition*, New York, NY, USA, 11-16 Nov. 2001.

[5] Wei Yang, "Microcombustion engine/generator," 1999, US Patent No.:6,276,313.

[6] A. G. Cooper, S.Kang, J. W. Kietzman, F. B. Prinz, J. L. Lombardi, and L. Weiss, "Automated Fabrication of Complex Molded Parts Using Mold SDM," in *Proceedings of the Solid Freeform Fabrication Symposium*, 1998.

[7] J.D. Denton, "Loss Mechanisms in Turbomachines," *Journal of Turbomachinery*, vol. 115, pp. 621–651, Oct. 1993.

[8] R. c. Pampreen, "Small Turbomachinery Compressor and Fan Aerodynamics," *ASME Journal of Engineering For Power*, vol. 95, pp. 215, 1971.

[9] B Eckert and E. Schnell, *Axial- und Radial-Kompressoren*, pp. 192–357, Springer Verlag, 2nd ed. edition, 1961.

[10] Pfleiderer, *Die Kreisel Pumpen*, p. 99, Springer-Verlag, 1961.

[11] S. Kang, *Fabrication of functional mesoscopic ceramic parts for micro gas turbine engine*, Ph.D. thesis, Stanford University, 2001.

[12] K. Isomura, "Feasibility Study of a Micromachined Gas Turbine," in *Workshop on Power MEMS, International Symposium on Research and Education in the 21st Century (ISRE2000)*, 2000.

[13] Scott B. Lattime and Bruce M. Steinetz, "Turbine engine clearance control systems: Current practices and future directions," in *38th AIAAASMESAEASEE Joint Propulsion Conference & Exhibit*, Indianapolis, Indiana, July 7.-10. 2002.

[14] John P. Barranger and M.J. Ford, "Laser-optical blade tip clearance measurement system," *Journal of Engineering for Power, Transactions of ASME*, vol. 103, pp. 457–460, 1981.
[15] G.L. Poppel, D.T.F. Marple, and J.D. Kingsley, "Analysis, design, fabrication and testing of an optical tip clearance sensor (turbocompressor blade tips) [final report, jun. 1979 - jan. 1981]," Tech. Rep., NASA-CR-165265; NAS 1.26:165265; R81AEG215, 1981.
[16] I. Davinson, "Optical sensors and signal processing schemes for use on gas turbine engines," in *34th International Instrumentation Symposium*, Albuquerque, NM, 2-6 May 1988.
[17] I. Davinson, "Astigmatic turbine bladfe tip clearance sensor for gas turbine aero engines," in *SPIE*, Cannes, France, November 17-20 1987, vol. 863 Industrial optoelectronic measurement systems using coherent light, p. 60.
[18] H.S. Dhadwal, A. Mehmud, R. Khan, and A. Kurkov, "Integrated fiber optic light probe: measurement of static deflections in rotating turbomachinery.," *Review of Scientific Instruments*, vol. 67, no. 2, pp. 546–552, 1996.
[19] H.S. Dhadwal, A.P. Kurkov, and D.C. Janetzke, "Time-of-flight tip-clearance measurements," in *35th AIAA/ASME/SAE/ASEE Joint Propulsion Conference and Exhibit*, Los Angeles, CA, June 20-24 1999, vol. AIAA Paper 99-2134.
[20] D. Mueller, A.G. Sheard, S. Mozumdar, and E. Johann, "Capacitive measurement of compressor and turbine blade tip to casing running clearance," *Journal of Engineering for Gas Turbines and Power*, vol. 119, pp. 877–884, 1997.
[21] John P. Barranger, "An in-place recalibration technique to extend the temperature capability of capacitance-sensing, rotor-blade-tip-clearance measurement systems," in *Society of Automotive Engineers, Aerospace Meeting,*, San Diego, Calif., Nov. 27-30 1978, vol. SAE PAPER 781003, p. 14.
[22] Rosario N. Demers, "Compressor blade clearance measurement using capacitance and phase lock techniques," in *AGARD Advanced Instrumentation for Aero Engine Components*, Philadelphia, PA, USA, May 19-23 1986, vol. AGARD-CP-399, p. 10.
[23] A.G. Sheard, S.G. O'Donnell, and J.F. Stringfellow, "High temperature proximity measurement in aero and industrial turbomachinery," *Journal of Engineering for Gas Turbines and Power*, vol. 121, pp. 167–173, 1999.
[24] Garimella R. Sarma and John P. Barranger, "Capacitance-type blade-tip clearance measurement system using a dual amplifier with ramp/dc inputs and integration," *IEEE Transactions on Instrumentation and Measurement*, vol. 41, no. 5, pp. 674–678, 1992.
[25] D.P. Davidson, R.D. Derose, and A.J. Wennerstrom, "The measurement of turbomachinery stator-to-drum running clearances," Tech. Rep., ASME 83-GT-204, 1983.
[26] A.G. Sheard, G.C. Westerman, and B. Killeen, "An on-line calibration technique for improved blade by blade tip clearance measurement," in *Proceedings of the 38th International Instrumentation Symposium*, Las Vegas, NV, USA, Apr. 26-30 1992, pp. 31–51.
[27] George W. Hardigg., "Apparatus for measuring rotor blade vibrations," 1951, US Patent No.:2,575,710.
[28] Lawrence W. Langley., "Eddy current clearance transducing system," 1989, US Patent No.:4,847,556.
[29] Greg W. Terpay and Jr Zipfel, George G., "Measuring blade condition in a gas turbine engine using eddy-currents," in *Proceedings of the 9th International Conference on Adaptive Structures and Technologies*, Boston, MA, USA, Oct. 14-16 1999, pp. 71–80.
[30] John W. H. Chivers, "Microwave interferometer," 1982, US Patent No.:4359683.
[31] Sydney C. Woolcock and Edwin G. Brown., "Checking the location of moving parts in a machine," 1982, US Patent No.:4346383.
[32] L.C. Hall and B.E. Jones, "An investigation into the use of a cone-jet sensor for clearance and eccentricity measurement in turbomachinery," *Proc. Inst. Mech. Eng.*, vol. 190, no. 17, pp. 23–30, 1976.
[33] Takeshi Tagashira, Nanahisa Sugiyama, Yukio Matsuda, and Masakatsu Matsuki, "Measurement of blade tip clearance using an ultrasonic sensor," in *35th AIAA, Aerospace Sciences Meeting & Exhibit*, Reno, NV, USA, Jan. 6-9 1997, AIAA Paper 97-0165.
[34] J.W.H. Chivers, "A technique for the measurement of blade tip clearance in a gas turbine," in *AIAA/ASME/SAE/ASEE 25th Joint Propulsion Conference*, Monterey, Ca, July 10-12 1989, vol. AIAA PAPER 89-2916.
[35] John P. Barranger, "Low-cost fm oscillator for capacitance type blade tip clearance measurement system," Tech. Rep., NASA-TP-2746, 1987.
[36] John P. Barranger, "Study of the capacitance technique for measuring high-temperature blade tip clearance on ceramic rotors," Tech. Rep., NASA-TM-105978, 1993.
[37] Rosario N. Demers., "Compressor blade clearance measurement system," 1989, US Patent No.:4806848.
[38] Tibor Fabian, Sangkyun Kang, Fritz Prinz, and Georg Brasseur, "Capacitive blade tip clearance measurements for a micro gas turbine," in *Proceedings of Instrumentation and Measurement Technology Conference*, 21-23 May 2002, vol. 2, pp. 1011–1015.
[39] Ross Venook, Garry Gold, Bob Hu, and Greig Scott, "Autotuning electronics fog varactor tuned, flexible interventional rf coils," May 2002, p. 893.
[40] J. van Drecht, Meijer G.C.M., and P.C. de Jong, "Concepts for the design of smart sensors and smart signal processors and their application to psd displacement transducers," *Digest of Technical Papers, Transducers '91*, 1991.
[41] John R. Taylor, *An introduction to Error Analysis*, 2nd edition, 1997.

Tibor Fabian was born in Poprad, Slovakia, in 1972. He received the Dipl.-Ing. degree in electrical engineering (1998) and the doctoral degree in technical science (2004) from the Vienna University of Technology, Vienna, Austria. He was a Research Assistant at the Rapid Prototyping Laboratory at Stanford University, USA from 1999 to 2004. He is currently a Research Associate at the Rapid Prototyping Laboratory, Mechanical engineering Department, Stanford University. His research interests include portable power sources such as miniature gas turbines and miniature fuel cells.

Georg Brasseur (M'94 - SM'97) was born in Vienna, Austria, in 1953. He received the Dipl.-Ing. degree in electrical engineering and the doctoral degree in technical science from the Vienna University of Technology, Vienna, Austria, in 1979 and 1985, respectively. He was an Assistant Professor at the Vienna University of Technology, heading the research group Automotive Electronics from 1979 to 1998. At that time, he received the "venia docendi" on industrial electronics. Since 1999, he has been a Full Professor heading the Institute of Electrical Measurement and Measurement Signal Processing, Graz University of Technology, Graz, Austria. He is author or coauthor of over 100 technical papers and patents. His research interests focus on automotive sensors, capacitive sensing devices, analog circuit design, automotive electronics, and actuators.

Friedrich B. Prinz Since 1994, he has been the Rodney H. Adams Professor of Engineering, Stanford University, with dual appointments as Professor of the Departments of Mechanical Engineering and Materials Science and Engineering. From 1994 to 2003, he was Co-Director of the Alliance for Innovative Manufacturing (AIM) at Stanford. Before joining Stanford University in 1994, he had been on the faculty of Carnegie Mellon University, for nearly 14 years, and was Professor of Mechanical Engineering from 1987 to 1994, as well as Director of the Engineering Design Research Center (NSF-ERC) from 1989 to 1994. He has published over 100 papers, among which the recent ones focus on ionic conductivity at nanoscale, and on the performance of novel fuel cell structures.